THE JOURNAL OF PHYSICAL CHEMISTRY C

Article

pubs.acs.org/JPCC

UV/O_3 Generated Graphene Nanomesh: Formation Mechanism, Properties, and FET Studies

Da-Peng Yang,[†,‡,⊥] Xiansong Wang,[†,‡,⊥] Xiaojun Guo,[§] Xiao Zhi,[†,‡] Kan Wang,[†] Chao Li,[†,‡] Gaoshan Huang,[§] Guangxia Shen,*[,†,§] Yongfeng Mei,[∥] and Daxiang Cui*[,†,‡,§]

[†]Key Laboratory for Thin Film and Microfabrication Technology of the Ministry of Education, Research Institute of Micro/Nano Science and Technology, Shanghai Jiao Tong University, 800 Dongchuan Road, 200240 Shanghai, People's Republic of China

[‡]Key Laboratory for the Genetics of Developmental & Neuropsychiatric Disorders of Ministry of Education, Bio-X Center, Shanghai Jiao Tong University, Dongchuan Road 800, 200240 Shanghai, People's Republic of China

[§]Department of Electronic Engineering, Shanghai Jiao Tong University, 200433 Shanghai, People's Republic of China

[∥]Department of Materials Science, Fudan University, Shanghai, People's Republic of China

Supporting Information

ABSTRACT: The bandgap engineering of graphene is a challenging task for its potential application. Forming unique structures such as nanoribbons or nanomeshes is an effective way to open up a bandgap in graphene. In this work, a graphene nanomesh (GNM) was prepared through UV-mediated oxidation of a graphene oxide (GO) film at atmosphere. Atomic force microscopy (AFM) was used to track the evolution of the surface morphology of GO during the irradiation. It was observed that a nanoporous network structure was progressively produced in the basal plane, which can be attributed to the fact that highly reactive oxygen species preferentially attack sp^3 carbon-rich regions of the GO. In particular, the as-prepared GNM shows interesting semiconducting characteristics and photoluminescence (PL) phenomenon, which make it become a promising candidate for the use of electronics, optoelectronics, and biomedical engineering. Finally, the field-effect transistors (FETs) were fabricated using the as-prepared GNM as the active channel. The measured electrical characteristics indicate that the use of UV/O_3 is an available choice to open the bandgap of graphene and tune its properties for optoelectronics or biomedical applications.

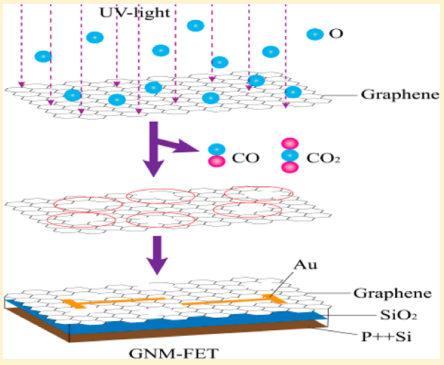

INTRODUCTION

Since the first discovery of monolayer graphene (mechanical exfoliation of graphite),[1] a great surge of research in graphene has emerged in different fields such as condensed-matter physics, material science, nanoelectronics, and biomedical engineering.[2−9] Graphene, which is made up of 100% sp^2-hybridized carbon atoms arranged in a honeycomb lattice, possesses a range of remarkable properties including high carrier mobility, thermal conductivity, high values of Young's modulus, and an anomalous quantum Hall effect.[8] These intriguing characteristics make graphene become a promising "star" material in the exploration of fundamental and application science.[9−12] However, due to the absence of energy bandgap, the potential applications in electronics, optoelectronics, and biomedical engineering are largely hindered.[13] Therefore, looking for effective ways to open up the bandgap is a challenging task.[14,15] Due to the influences of the quantum confinement, edge, and localization effects to graphene bandgap, great efforts have been devoted to tailoring graphene sheets into a confined geometry such as nanoribbons,[16−18] quantum dots,[19,20] and nanomeshes[21−23] or doping some heterogeneous atoms (O, N, and Mn) or molecules into the graphene parent material.[24−27] These well-designed structures are effective in tuning and controlling the semiconducting properties of graphene. In order to get these delicate structures, various approaches have been explored, such as lithography (including electron beam,[28] block copolymer,[20] and nanosphere[27]), ion irradiation,[29] hydrothermal,[30] template,[31] chemical vapor deposition,[32] photocatalytic reduction or oxidation,[33] plasma etching,[34] etc. Among these methods, oxidation is of particular interest not only from its technical advantages (easy operation, cost-effective, versatile design, and short reaction time) but also from a fundamental science perspective due to the oxygen involvement.[35,36] Elucidating how oxygen breaks into carbon world could stimulate the development of a new area of nanotechnology based on nanoscale graphite origami.[37] Previously, the oxidation of graphene has been explored by some researchers. For example, Solís-Fernández et al. systematically investigated the oxidation behavior of reduced graphene oxide (rGO) by thermal oxidation in air, microwave oxygen plasma, and ultraviolet-generated ozone.[9,10,38] Later, Tao et al. reported the morphology of graphene sheets treated in an

Received: October 5, 2013
Revised: December 6, 2013
Published: December 10, 2013

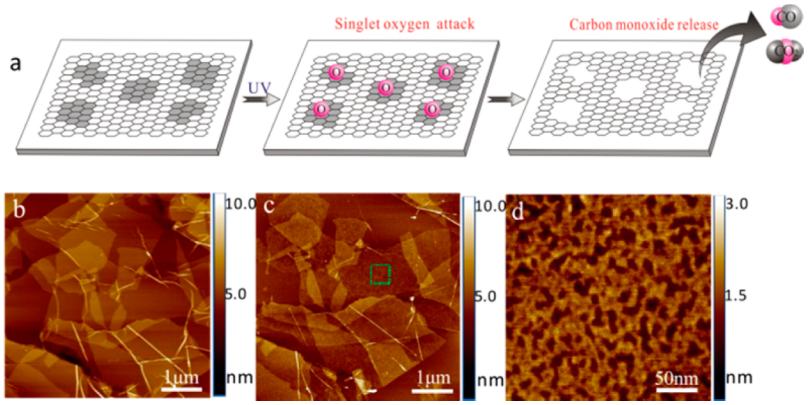

Figure 1. (a) Schematic illustration of the UV exposure process of GO to form a perforated GNM. First, GO solution was deposited onto the freshly prepared mica sheet surface (1.0 × 1.0 cm^2) and dried in the vacuum oven. Then, the dried substrates were put into a sealed box with UV irradiation. Note: the dark gray areas represent sp^3 carbon clusters and the remaining regions are sp^2 carbon domains. (b–d) AFM images of GO sheets on the mica substrate: (b) the starting GO sheets, (c) the UV-irradiated GO, and (d) zoom-in of a square region; see (c) showing the perforated structure of an individual sheet.

ozone generator.[39] However, their work mainly focused on the morphology changes and formation process discussions. A fully comprehensive, systematic study of formation mechanism and optoelectrical properties is still missing. In fact, after UV/ozone oxidation, an electron energy gap in graphene could be opened and its properties might give rise to some remarkable changes. For example, Huh et al. reported that ozone molecules could react with graphene to produce oxygen-containing groups and induce the p-type doping of the graphene.[40−43] Such structure can be used as a highly Raman-active substrate for SERS sensing applications.[44] Gokus et al. induced the strong photoluminescence (PL) in single-layer graphene by oxygen plasma treatment.[45−48] In this study, we fully used the processing advantages and unique properties of graphene oxide (GO) and utilized UV/ozone to oxidize/etch GO in a sealed chamber; a detailed analysis of the evolution process regarding the morphology characteristics of GO with different exposure time (1, 3, and 5 min) was observed by AFM. After 5 min exposure, it is found that a nanoporous structure (called graphene nanomesh, GNM) was produced in the basal plane. XPS and Raman experiments were also performed to reveal the structural changes before and after exposure. Subsequently, the optoelectronic properties of GNM were also tested. Finally, the field-effect transistors (FETs) were fabricated using the GNM as the active channel and characterized.

EXPERIMENTAL SECTION

Materials. Reagent grade chemicals were purchased from Aldrich. Graphitic powder (500 mesh) was purchased from Beijing Chemical Reagents.

Preparation of Graphene Nanomesh. Graphene oxide (GO) was first produced through a modified Hummer's method by reacting natural graphite powder in a mixture of $NaNO_3$, H_2SO_4, and $KMnO_4$.[8−10] After the reaction, H_2O_2 was added to the system. The yellow suspension was filtered and washed for three times using HCl and then dispersed in deionized H_2O. The homogeneous graphene oxide dispersions were obtained by sonicating the graphite oxide suspension at room temperature for 1 h. GO dispersion in water was deposited onto the freshly prepared mica sheet surface (1.0 × 1.0 cm^2) and dried in a vacuum oven at 60 °C. Subsequently, the dried sample was put into a 25.4 cm i.d. Rayonet photochemical chamber equipped with Hg lamps. The Hg lamps were designed to emit 184.9 and 253.7 nm photons. The irradiation experiment was carried out at atmosphere.

Characterization of Graphene Nanomesh. Atomic force microscopy (AFM) measurements were performed in tapping mode on a multimode nanoscope V scanning probe microscopy system (Veeco Instruments).[44] Commercially available AFM cantilever tips with a force constant of ∼48 N m^{-1} and resonance vibration frequency of ∼330 kHz were used. Photoelectron spectroscopy (XPS) measurements were carried out on an Axis Ultra DLD X-ray photoelectron spectroscope (Kratos Analytical, UK) using a monochromatic Al Kα (1486.6 eV) source at 15 kV. Raman measurements were performed on an Invia/Reflrx Lasser Micro-Raman spectroscope (Reinshaw, England) with excitation laser beam wavelength of 514 nm. Pristine GO or UV-irradiated GO were placed on a clean mica sheet. Electrical conducting measurements of individual GO, r-GO, and graphene nanomesh were performed using a two-electrode system based on conductive atomic force microscopy (C-AFM). PL measurement was carried out using a fluorescence microscope (Olympus IX71) equipped with a multispectral imaging system (Caliper CRi Nuance). The GO and GNM samples were coated on glass sheet with a layer of thickness of 10 nm. Then, the sample was put under the inverted florescence microscope to be observed.

Construction and Property Measurement of FET Devices. GNM-based FET devices were fabricated on a Si/SiO_2 (300 nm) wafer. The Au electrodes were defined by thermal evaporation for 2 h through a shadow mask with the channel width (W) of 1200 μm and the length (L) of 80 μm. The current–voltage (I–V) curves were characterized by Keithley 4200 semiconductor characterization system under ambient and dark conditions. We employ density functional theory in the generalized gradient approximation implemented in the Quantum-ESPRESSO package. Perdew–Burke–Ernzerhof norm-conserving pseudopotentials are used. We find that a 5 × 5 × 1 surpercell of pristine graphene is sufficiently large for our calculations. The supercell with a lattice constant of a = 12.2 Å contains 50 carbon atoms. All calculations are performed with a plane wave cutoff energy of 544 eV and a 4 × 4 × 1 k-mesh for the Brillouin zone integration. Interlayer interactions due to the periodic boundary conditions are prevented by a vacuum slab of ∼20 Å thickness. The atomic positions are fully

dx.doi.org/10.1021/jp409898d | J. Phys. Chem. C 2014, 118, 725−731

relaxed in all cases until an energy convergence of 10^{-7} eV and a force convergence of 0.05 eV/Å are reached.

RESULTS AND DISCUSSION

Preparation of Graphene Nanomesh. The overall strategy of punching holes on the GO to form GNM is schematically displayed in Figure 1a. First, solution-phase prepared water-dispersible GO deposited on mica was employed as the starting material. Inherited from the preparation process, GO is highly oxidized, bearing hydroxyl and epoxide functional groups forming sp^3 bonds with carbon atoms on their basal planes. The sp^3 bonded carbon clusters with irregular sizes and shapes (Figure 1a, gray region) are embedded in the sp^2 carbon network. Upon UV irradiation, some highly reactive oxygen species are created in the photochemical cell.[39] Initially, the preferred attacking site is located on sp^3 carbon clusters or defective regions. The oxygenation leads to the release of CO and CO_2 in sp^3 carbon-rich regions, leaving behind a porous sp^2 carbon percolating network structure.

Characterization of Graphene Nanomesh. Atomic force microscopy (AFM) was employed to observe the change of a single GO sheet before and after UV irradiation. Figure 1b is the AFM image of the untreated GO sheets which show the clean and smooth surfaces. After 5 min UV exposure, as shown in Figure 1c, lots of pits are observed on the heavily roughened surfaces. However, their sizes are not apparently reduced, and no global fracturing or curling behavior occurs. Meanwhile, it seems that the local cracks are not triggered from the edges. The same phenomenon was previously reported for hydrothermal steaming of GO sheets, assuming that the edges of the GO sheets are not more reactive sites than the basal planes.[40] Therefore, UV/O_3 etching of GO sheets can disrupt their structures, likely to initiate from the more defective sp^3-rich domains. This is also identified by UV−vis spectra, showing that the electronic conjugation was restored upon UV/O_3 etching (Figure S1). Figure 1d is the magnified image of a square area on an individual GO sheet. As can be seen, the shapes and sizes of cracking regions are irregular, with an average width of 20 nm. The remaining parts (particulate domains) are interconnected to form the nanoporous network.

To better understand the evolution of GO sheets exposed to UV, we carried on with a more detailed AFM study on an individual GO sheet for different irradiation times. Figures 2a−c show typical AFM images of the morphological evolution at room temperature after the exposure of 1, 3, and 5 min, respectively. For the shortest exposure time (1 min, Figure 2a), the morphology is similar to the untreated GO sheet as shown in Figure S2. However, a slight increase of the corrugation occurred in Figure 2a, reflecting the starting interaction of oxygen species with the surface of GO at 1 min. After 3 min of exposure, the morphology gives rise to notable changes with lots of pits formed through the whole sheet as shown in Figure 2b. After 5 min of exposure (Figure 2c), more pits occur on the surface and become much deeper than observed in Figure 2b. Compared with the height profiles shown in Figure 2d for three different exposure time (1, 3, and 5 min), we find that the average thickness for 1 min exposure is ca. 1.0 nm, which matches well with the thickness of untreated GO sheet (Figure S2, the height profile). However, the height profile changes greatly after 3 min exposure, with the average thickness of the sheet decreasing to 0.3−0.5 nm, showing a great number of dangling C−O bonds have been eliminated for the extending

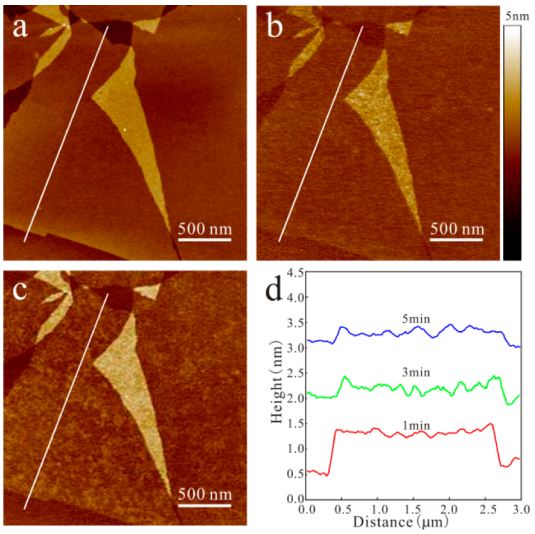

Figure 2. In-situ tapping mode AFM images and height profiles (superimposed on the images) showing the evolution of a perforated GNM on the mica surface for different UV illumination times: (a) 1, (b) 3, and (c) 5 min. (d) Representative height profiles taken along the marked white lines.

exposure. This apparent height change is further proved for 5 min exposure in which the average thickness of the sheet is ca. 0.3 nm, and some points even are near to 0 nm. It is worth noting that the thickness of an ideal monolayer of graphene is ~0.34 nm. According to this fact, we assume that the initial sp^3 carbon-rich "islands" nonhomogeneously distributed in the sp^2 carbon "ocean" were etched off during the UV irradiation process, leaving behind a sp^2 carbon interconnecting network structure in our terminal product. On the basis of this assumption, on one hand, we can elucidate the height profile changes corresponding to different irradiation times; on the other hand, the formation of GNM can also be given a reasonable explanation due to sp^3 carbon etching. Considering the participation of oxygen species in the reaction, the disappearing sp^3 regions may have escaped as CO and CO_2 (Figure S3). This has been proved experimentally that ozone-reacted CNTs (SWCNTs) containing surface-bond functional groups such as C═O, C═C, and C−O could release gas phase CO_2 and CO under a heat treatment ($T > 473$ K) of UV/O_3.[41]

Although the exact chemical structure of GO is not well established, it is believed that a variety of oxygen-containing functional groups (such as epoxide and hydroxyl groups on the interior of the sheet and carbonyl groups at the edges) could become the active sites as similar as the ozone-reacted CNTs. Raman spectroscopy was further used to study the structural information on GO and GNM. The D and G peaks are two important features which reflect the ordered/disordered crystal structures of carbonaceous materials. The G band (corresponds to the E_{2g} phonons of the sp^2 C−C bonds) is caused by bond stretching of sp^2 carbon pairs in both rings and chins, while the D band (corresponds to the breaking mode of κ-point phonons of A_{1g} symmetry) is generated by local defects and disorder.[42,43] Therefore, the I_D/I_G ratio can be regarded as a measure of the amount of disorder present within the materials.[31] Typical Raman spectra of monolayers of GO and the GNM obtained at an excitation wavelength of 532 nm are shown in Figure 3a. The D and G bands are located at about 1350 and 1600 cm^{-1}, respectively. The I_D/I_G ratio increases from 0.66 for GO to 0.79

dx.doi.org/10.1021/jp409898d | J. Phys. Chem. C 2014, 118, 725−731

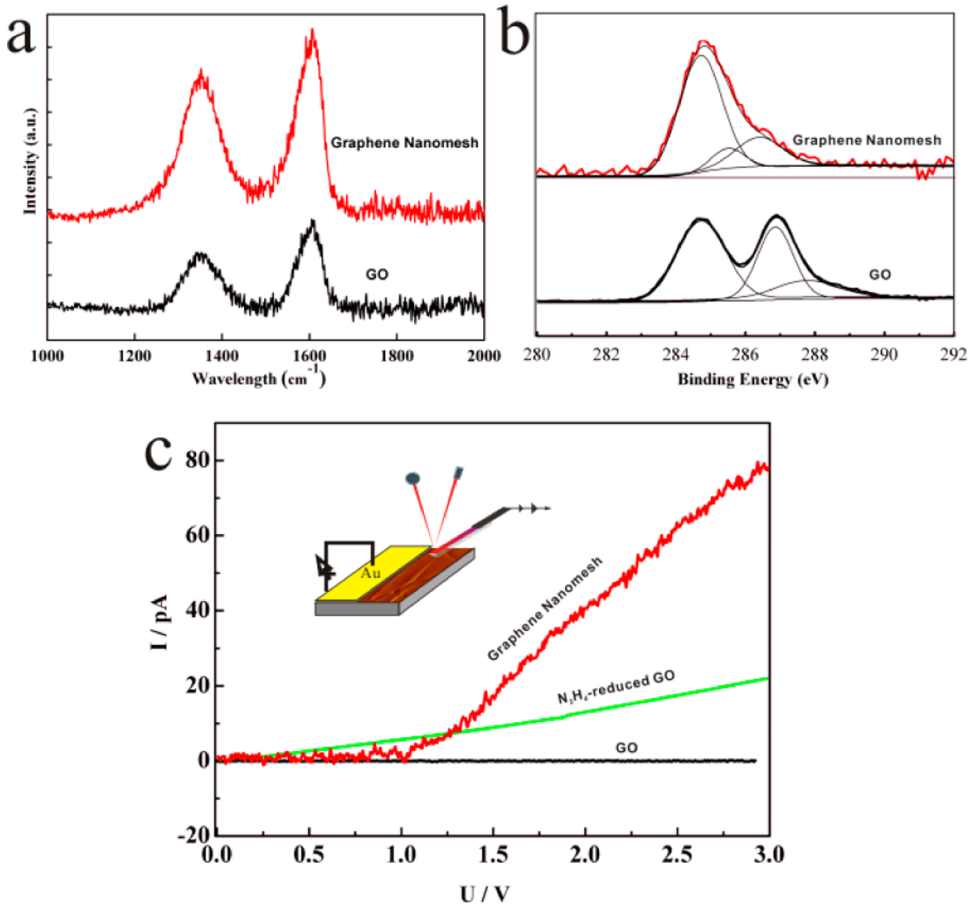

Figure 3. (a) Raman spectra of GO (black) and the corresponding perforated GNM (red) with 5 min UV exposure. Note: D peak/G peak = 0.66 for GO; in contrast, D peak/G peak = 0.79 for the GNM. Therefore, the ratio of D/G is evidently increased, showing that more disorders and defects generated. After UV illumination for 5 min, the newly formed sp^2 clusters are connected so that transport by percolation might occur. (b) X-ray photoelectron spectroscopy (XPS) spectra in C 1s of GO (black) and GNM (red), showing that after UV illumination for 5 min, the C 1s peaks of oxygen-containing groups were decreased largely. (c) Electrical properties of GO-based devices on mica. Current−voltage curves measured by using conductive atomic force microscopy (C-AFM) for three different types of devices: as-prepared GO (black), N_2H_4-reduced GO (green), and GNM (red). Note: over 10 devices have been measured for each of the three states. The inset shows a schematic illustration of a two-electrode system.

for the GNM, indicating the more defects and disorder occurred due to the UV irradiation. The defects can be attributed to the formation of pores in the GNM as seen in the AFM images. Although the Raman spectrum can detect small changes in the crystal structure, the change of chemical composition remains unclear. In order to clarify the changes of the surface chemical state of the GO sheets and GNM, XPS was utilized. Figure 3b shows the deconvoluted C1S XPS spectra of the pristine GO sheets. The signal at 284.5 eV corresponds to C−C bonds, while the signals in the range of 286−289 eV are assigned to C−O bonds. The ratio of C/O is 1.52. After UV irradiation, the peaks of the C−C bonds are strongly increased in intensity, while the peaks of the C−O bonds decline significantly, as shown in Figure 3b. Note that the ratio of C/O increases to 5.23, suggesting that the most oxygen-containing groups have already been removed, leaving behind a predominant sp^2 carbon cluster interconnected network. The XPS C 1s spectrum can partially support our deduction that oxygen can leave in the form of CO and CO_2.

As the properties of GO are largely depended on the structure and chemical composition,[6] in other words, due to UV-mediated oxidation disruption, the newly arranged π-electrons of the sp^2 carbon on the GNM will particularly affect its optoelectronic characteristics.[44−46] Importantly, density functional theory study indicates that a low oxidation on GO will yield a small band gap which gives GO a semiconducting behavior.[48−51] These previous analysis prompted us to investigate the electrical conductivity and photoluminescence toward graphene bandgap engineering.[44−47] For comparison, the electronic properties of pristine GO, hydrazine reduced GO, and UV-treated GO were studied by building a two-electrode system based on conductive atomic force microscopy (C-AFM). C-AFM is very useful for the measurement of high resistivity films. The principles are schematically shown in the insets of Figure 3c. To perform C-AFM measurement, a selectable bias between the GO sample and the conductive SPM tip virtually on ground was applied (Figure 3c, schematic inset). As the conducting tip is scanning the GO sample in contact mode and imaging the topography, a linear amplifier with a range of 1 pA to 1 μA senses the current passing through the GO sample. Thus, the sample's topography and current image are measured simultaneously, enabling the direct correlation of the location with electrical properties. Pristine GO has a sheet resistance (R_s) values of about 1012 Ω sq^{-1} or higher, thus showing an insulating nature (see Figure 3c). Owing to the high number of oxygen-containing functional groups present on the surface, the pathways among the sp^2 carbon clusters can be blocked, inhibiting carrier transport.[46]

dx.doi.org/10.1021/jp409898d | J. Phys. Chem. C 2014, 118, 725−731

However, the conductivity can be enhanced by N_2H_4 reduction. This could be due to the preferential attack of hydrazine to oxygen-containing groups, leading to partial restoration of the sp^2-conjugated graphene network. Conversely, the GNM formed by UV-mediated oxidation shows a semiconducting nature. In view of the above results and discussions, we believe that approximate oxidation eliminates the sp^3 carbon domains and forms a percolating network of sp^2 carbon which is beneficial to carrier mobility.

In addition, microscopic structural defects/disorders may also influence the conductivity of the GNM. On the other hand, photoluminescence (PL) spectroscopy was also measured to prove that the bandgap opening of GNM through UV/O_3 treatment. Room temperature imaging and PL were carried out on GNM using 400, 455, and 570 nm excitation wavelengths and a CCD spectrometer. The solid GNM shows two different PL characters (green and red light) as observed in Figure 4a–c.

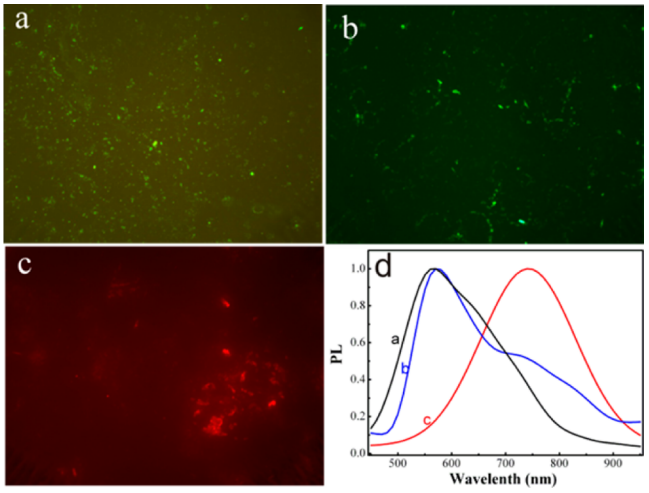

Figure 4. Fluorescence microscopic imaging (×100) and corresponding PL spectrum of GNM with three different excitation wavelengths (400, 455, and 570 nm).

It seems that the photoluminescent areas are made up of some incontinuous dots with different sizes and intensity. Combined with our AFM observation, we deduce that these PL carbon dots are likely derived from the isolated sp^2 carbon parts on GNM. Correspondingly, three distinct PL peaks (collected on individual PL dot) at the maximum wavelengths of 550, 560, and 760 nm are measured, as shown in Figure 4d. Obviously, the emission maximum shifted with increasing excitation wavelengths; PL carbon dots should be responsible for this phenomenon. The photoluminescence could be attributed to the electron-confined sp^2 islands (its shape, size, and ratio of sp^2/sp^3 carbon),[46,47] it is more likely to arise from UV/O_3 oxidative etching as described in Figure 1. Our results also show that the UV/O_3 oxidative etching method can be used for preparation of PL carbon dots; their collection and application for biomedical engineering are under way, which will be reported in another paper.

Construction and Property Measurement of FET Devices. Considering the conducting property of the obtained GNM, after characterizing the chemical and physical structures of GNM, we then used it as the active channel to fabricate FET devices (Figure S4), with a heavily doped Si as the gate, a 300 nm thick SiO_2 layer as the gate dielectric, and thermally evaporated Au as the source and drain electrodes (Figure 5a).

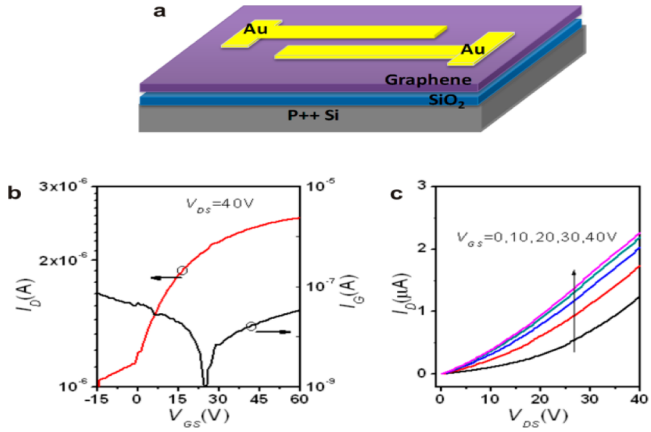

Figure 5. Room temperature electrical properties of a GNM device. (a) Schematic illustration of a GNM-FET. The device is fabricated on a heavily doped silicon substrate with 300 nm SiO_2 as the gate insulator layer. (b) The measured transfer characteristics (I_D–V_{GS}) and gate leakage as a function of the gate bias (I_G–V_{GS}) of the GNM FET. (c) The output characteristics (I_D–V_{DS}) of the GNM FET at the gate bias from 0 to 40 V with the step of 10 V.

80 nm thick Au source and drain electrodes were prepared by thermal evaporation through a shadow mask to define the channel width of 1200 μm and the length of 80 μm.[42−44] The electronic characterization of the FET devices was carried out under ambient and dark conditions. Figures 5b and 5c show the measured transfer (I_D–V_{GS}) and output (I_D–V_{DS}) electrical characteristics, respectively, which indicate n-type transistor behaviors. The ON/OFF current ratio is about 2.5. The measured gate leakage (I_G) as a function of the gate bias (V_{GS}) is also shown in Figure 5b to prove that the measured drain current (I_D) modulated by the gate bias (V_{GS}) is mainly contributed by the channel, and therefore it can be confirmed that the GNM prepared through UV-mediated oxidation of a GO film presents the semiconducting properties.

CONCLUSIONS

In conclusion, we have utilized UV/O_3 to build up a nanoporous, electrically conductive GNM. The approach is simple, scalable, energy efficient, and controllable. During the UV irradiation, oxygen species produced in the air (mainly singlet oxygen) are efficient attackers to sp^3 carbon domains on GO. The components of the attacked sites are taken away in the form of CO and CO_2, giving rise to a percolating network which is mainly made up of sp^2 carbon clusters. The resulting product (GNM) shows interesting electronic and optical characteristics, forming an exciting platform to study GO-based nanodevice application. The semiconducting property is also confirmed by electrical measurements on a back-gated FET device. Moreover, the established oxidation mechanism is useful to understand the atomic-level mechanisms of oxidation in carbon-based materials. We believe that the UV/O_3 generated GNM is one kind of promising carbon-based material and owns great potential in applications such as optoelectric devices and biosensors as well as biomedical engineering in the near future.

ASSOCIATED CONTENT

Supporting Information

Figures S1–S4. This material is available free of charge via the Internet at http://pubs.acs.org.

dx.doi.org/10.1021/jp409898d | J. Phys. Chem. C 2014, 118, 725–731

AUTHOR INFORMATION

Corresponding Authors

*E-mail dxcui@sjtu.edu.cn (D.C.).
*E-mail gxshen@sjtu.edu.cn (G.S.).

Author Contributions

⊥D.-P.Y. and X.W. contributed equally.

Notes

The authors declare no competing financial interest.

ACKNOWLEDGMENTS

We thank Dr. Yingchun Cheng (King Abdullah University of Science and Technology, Kingdom of Saudi Arabia) for the calculative parts. This work is supported by the China Nano 973 project (No. 2010CB933902), National Natural Scientific Fund of China (No. 81225010, 31100717), 863 project of China (2012AA022703), and Shanghai Science and Technology Fund (No. 13 nm1401500 and 11 nm0504200).

REFERENCES

(1) Novoselov, K.; Geim, A.; Morozov, S.; Jiang, D.; Zhang, Y.; Dubonos, S.; Grigorieva, I.; Firsov, A. Two-dimensional gas of massless Dirac fermions in graphene. *Science* **2004**, *306*, 666.

(2) (a) Geim, A. K.; Novoselov, K. S. The rise of graphene. *Nat. Mater.* **2007**, *6*, 183. (b) Huang, X.; Zeng, Z. Y.; Fan, Z. X.; Liu, J. Q.; Zhang, H. Graphene-based electrodes. *Adv. Mater.* **2012**, *24*, 5979.

(3) (a) Allen, M. J.; Tung, V. C.; Kaner, R. B. Honeycomb carbon: a review of graphene. *Chem. Rev.* **2010**, *110*, 132. (b) Huang, X.; Qi, X.; Boey, F.; Zhang, H. Graphene-based composites. *Chem. Soc. Rev.* **2012**, *41*, 666.

(4) Geim, A. K. Graphene: status and prospects. *Science* **2009**, *324*, 1530.

(5) Wei, Z. Q.; Wang, D. B.; Kim, S.; Kim, S. Y.; Hu, Y.; Yakes, M. K.; Laracuente, A. R.; Dai, Z. T.; Marder, S. R.; Berger, C. Nanoscale tunable reduction of graphene oxide for graphene electronics. *Science* **2010**, *328*, 1373.

(6) Eda, G.; Chhowalla, M. Chemically derived graphene oxide: towards large-area thin-film electronics and optoelectronics. *Adv. Mater.* **2010**, *22*, 2392.

(7) Huang, X.; Yin, Z.; Wu, S.; Qi, X.; He, Q.; Zhang, Q.; Yan, Q.; Boey, F.; Zhang, H. Graphene-based materials: synthesis, characterization, properties, and applications. *Small* **2011**, *7*, 1876.

(8) Wu, X. Y.; Zhang, Y.; Wu, X. C.; Yang, Y. Q.; Zhou, X. J.; Wu, H. X. Biological applications of graphene and graphene oxide. *Nano Biomed. Eng.* **2012**, *4*, 157−162.

(9) Cheng, J. S.; Liang, Q. Q.; Chang, H. X.; Zhu, W. J. Redox approaches derived tin (IV) oxide nanoparticles/graphene nanocomposites as the near-infrared absorber for selective human prostate cancer cells destruction. *Nano Biomed. Eng.* **2012**, *4*, 76−82.

(10) Huang, P.; Xu, C.; Lin, J.; Wang, C.; Wang, X.; Zhang, C.; Zhou, X.; Guo, S.; Cui, D. X. Folic Acid-conjugated graphene oxide loaded with photosensitizers for targeting photodynamic therapy. *Theranostics* **2011**, *1*, 240−250.

(11) Li, C.; Wang, X. S.; Chen, F.; Zhang, C. L.; Zhi, X.; Wang, K.; Cui, D. X. The antifungal activity of graphene oxide silver nanocomposites. *Biomaterials* **2013**, *34*, 3882−3890.

(12) Wang, K.; Ruan, J.; Song, H.; Zhang, J. L.; Wo, Y.; Guo, S. W.; Cui, D. X. Biocompatibility of graphene oxide. *Nanoscale Res. Lett.* **2011**, *6*, 8.

(13) Novoselov, K.; Geim, A. K.; Morozov, S.; Jiang, D.; Grigorieva, M. I.; Dubonos, S.; Firsov, A. Two-dimensional gas of massless Dirac fermions in graphene. *Nature* **2005**, *438*, 197.

(14) Han, M. Y.; Özyilmaz, B.; Zhang, Y.; Kim, P. Energy band-gap engineering of graphene nanoribbons. *Phys. Rev. Lett.* **2007**, *98*, 206805.

(15) Jia, X.; Campos-Delgado, J.; Terrones, M.; Meunier, V.; Dresselhaus, M. S. Graphene edges: a review of their fabrication and characterization. *Nanoscale* **2011**, *3*, 86.

(16) Kosynkin, D. V.; Higginbotham, A. L.; Sinitskii, A.; Lomeda, J. R.; Dimiev, A.; Price, B. K.; Tour, J. M. Longitudinal unzipping of carbon nanotubes to form graphene nanoribbons. *Nature* **2009**, *458*, 872.

(17) Jiao, L.; Zhang, L.; Wang, X.; Diankov, G.; Dai, H. Narrow graphene nanoribbons from carbon nanotubes. *Nature* **2009**, *458*, 877.

(18) Cai, J.; Ruffieux, P.; Jaafar, R.; Bieri, M.; Braun, T.; Blankenburg, S.; Muoth, M.; Seitsonen, A. P.; Saleh, M.; Feng, X. Atomically precise bottom-up fabrication of graphene nanoribbons. *Nature* **2010**, *466*, 470.

(19) Yan, X.; Cui, X.; Li, L. S. Synthesis of large, stable colloidal graphene quantum dots with tunable size. *J. Am. Chem. Soc.* **2010**, *132*, 5944.

(20) Liu, R.; Wu, D.; Feng, X.; Müllen, K. Bottom-up fabrication of photoluminescent graphene quantum dots with uniform morphology. *J. Am. Chem. Soc.* **2011**, *133*, 15221.

(21) Bai, J.; Zhong, X.; Jiang, S.; Huang, Y.; Duan, X. Graphene nanomesh. *Nat. Nanotechnol.* **2010**, *5*, 190.

(22) Akhavan, O. Graphene nanomesh by ZnO nanorod photocatalysts. *ACS Nano* **2010**, *4*, 4174.

(23) Liang, X. G.; Jung, Y. S.; Wu, S. W.; Ismach, A.; Olynick, D. L.; Cabrini, S.; Bokor, J. Formation of bandgap and subbands in graphene nanomeshes with sub-10 nm ribbon width fabricated via nanoimprint lithography. *Nano Lett.* **2010**, *10*, 2454.

(24) Liu, H.; Liu, Y.; Zhu, D. Chemical doping of graphene. *J. Mater. Chem.* **2011**, *21*, 3335.

(25) Zhang, W.; Lin, C. T.; Liu, K. K.; Tite, T.; Su, C. Y.; Chang, C. H.; Lee, Y. H.; Chu, C. W.; Wei, K. H.; Kuo, J. L.; Li, L. J. Opening an electrical band gap of bilayer graphene with molecular doping. *ACS Nano* **2011**, *5*, 7517.

(26) Gan, Z. X.; Xiong, S. J.; Wu, X. L.; He, C. Y.; Shen, J. C.; Chu, P. K. Mn^{2+}-bonded reduced graphene oxide with strong radiative recombination in broad visible range caused by resonant energy transfer. *Nano Lett.* **2011**, *11*, 3951.

(27) Guo, B.; Liu, Q.; Chen, E.; Zhu, H. W.; Fang, L.; Gong, J. R. Controllable N-doping of graphene. *Nano Lett.* **2010**, *10*, 4975.

(28) Zhi, X.; Fang, H. L.; Bao, C. C.; Shen, G. X.; Zhang, J. L.; Wang, K.; Guo, S. W.; Wan, T.; Cui, D. X. The immunotoxicity of graphene oxides and the effect of PVP-coating. *Biomaterials* **2013**, *34*, 5254−5261.

(29) Cong, C. X.; Yu, T.; Ni, Z. H.; Liu, L.; Shen, Z. X.; Huang, W. Fabrication of graphene nanodisk arrays using nanosphere lithography. *J. Phys. Chem. C* **2009**, *113*, 6529.

(30) Tapaszto, L.; Dobrik, G.; Nemes-Incze, P.; Vertesy, G.; Lambin, P.; Biro, L. P. Tuning the electronic structure of graphene by ion irradiation. *Phys. Rev. B* **2008**, *78*, 233407.

(31) Pan, D.; Zhang, J.; Li, Z.; Wu, M. Hydrothermal route for cutting graphene sheets into blue-luminescent graphene quantum dots. *Adv. Mater.* **2010**, *22*, 734.

(32) Zeng, Z.; Huang, X.; Yin, Z.; Li, H.; Chen, Y.; Zhang, Q.; Ma, J.; Boey, F.; Zhang, H. Fabrication of graphene nanomesh by using an anodic aluminum oxide membrane as a template. *Adv. Mater.* **2012**, *24*, 4138.

(33) Zhang, Y.; Li, Z.; Kim, P.; Zhang, L.; Zhou, C. Anisotropic hydrogen etching of chemical vapor deposited graphene. *ACS Nano* **2011**, *6*, 126.

(34) Zhang, L.; Diao, S.; Nie, Y.; Yan, K.; Liu, N.; Dai, B.; Xie, Q.; Reina, A.; Kong, J.; Liu, Z. Photocatalytic patterning and modification of graphene. *J. Am. Chem. Soc.* **2011**, *133*, 2706.

(35) Zhou, X. Z.; Lu, G.; Qi, X. Y.; Wu, S. X.; Li, H.; Boey, F.; Zhang, H. A method for fabrication of graphene oxide nanoribbons from graphene oxide wrinkles. *J. Phys. Chem. C* **2009**, *113*, 19119.

(36) Liu, L.; Ryu, S.; Tomasik, M. R.; Stolyarova, E.; Jung, N.; Hybertsen, M. S.; Steigerwald, M. L.; Brus, L. E.; Flynn, G. W. Graphene oxidation: thickness-dependent etching and strong chemical doping. *Nano Lett.* **2008**, *8*, 1965.

(37) Li, J. L.; Kudin, K. N.; McAllister, M. J.; Prud'homme, R. K.; Aksay, I. A.; Car, R. Oxygen-driven unzipping of graphitic materials. *Phys. Rev. Lett.* **2006**, *96*, 176101.
(38) Ajayan, P. M.; Yakobson, B. I. Material science:oxygen breaks into carbon world. *Nature* **2006**, *441*, 818.
(39) Solís-Fernández, P.; Paredes, J.; Villar-Rodil, S.; Guardia, L.; Fernández-Merino, M.; Dobrik, G.; Biró, L.; Martínez-Alonso, A.; Tascón, J. Global and Local Oxidation behavior of reduced graphene oxide. *J. Phys. Chem. C* **2011**, *115*, 7956.
(40) Tao, H.; Moser, J.; Alzina, F.; Wang, Q.; Sotomayor-Torres, C. M. The morphology of graphene sheets treated in an ozone generator. *J. Phys. Chem. C* **2011**, *115*, 18257.
(41) Parekh, B.; Debies, T.; Knight, P.; Santhanam, K.; Takacs, G. Surface functionalization of multiwalled carbon nanotubes with UV and vacuum UV photo-oxidation. *J. Adhes Sci. Technol.* **2006**, *20*, 1833.
(42) Gokus, T.; Nair, R.; Bonetti, A.; Bohmler, M.; Lombardo, A.; Novoselov, K.; Geim, A.; Ferrari, A.; Hartschuh, A. Making graphene luminsecent by oxygen plasma treatment. *ACS Nano* **2009**, *3*, 3963.
(43) Huh, S.; Park, J.; Kim, Y. S.; Kim, K. S.; Hong, B. H.; Nam, J. M. UV/Ozone-oxidized large-scale graphene platform with large chemical enhancement in surface-enhanced Raman scattering. *ACS Nano* **2011**, *5*, 9799.
(44) Wang, X. S.; Yang, D. P.; Huang, G. S.; Huang, P.; Shen, G. X.; Guo, S. W.; Mei, Y. F.; Cui, D. X. Rolling up graphene oxide sheets into micro/nanoscrolls by nanoparticle aggregation. *J. Mater. Chem.* **2012**, *22*, 17441−17444.
(45) Radich, J. G.; Kamat, P. V. Making graphene holey. Gold-nanoparticle-mediated hydroxyl radical attack on reduced graphene oxide. *ACS Nano* **2013**, *7*, 5546−5557.
(46) Kamat, P. V.; Tvrdy, K.; Baker, D. R.; Radich, J. G. Beyond photovoltaics: semiconductor nanoarchitectures for liquid-junction solar cells. *Chem. Rev.* **2010**, *110*, 6664−6688.
(47) Huang, P.; Lin, J.; Wang, X. S.; Wang, Z.; Zhang, C. L.; He, M.; et al. Light-triggered theranostics based on photosensitizer-conjugated carbon dots for simultaneous enhanced-fluorescence imaging and photodynamic therapy. *Adv. Mater.* **2012**, *24*, 5104−5110.
(48) Mawhinney, D. B.; Naumenko, V.; Kuznetsova, A.; Yates, J.; Liu, J.; Smalley, R. Infrared spectral evidence for the etching of carbon nanotubes: ozone oxidation at 298 K. *J. Am. Chem. Soc.* **2000**, *122*, 2383.
(49) Wang, X. S.; Huang, P.; Feng, L. L.; He, M.; Guo, S. W.; Shen, G. X.; Cui, D. X. Green controllable synthesis of silver nanomaterials on graphene oxide sheets via spontaneous reduction. *RSC Adv.* **2012**, *2*, 3816−3822.
(50) Ferrari, A.; Robertson, J. Interpretation of Raman spectra of disordered and amorphous carbon. *Phys. Rev. B* **2000**, *61*, 14095.
(51) Lahaye, R.; Jeong, H.; Park, C.; Lee, Y. Density functional theory study of graphite oxide for different oxidation levels. *Phys. Rev. B* **2009**, *79*, 125435.